PAPER

Solution processable high-performance infrared organic photodetector by iodine doping †

Received 00th January 20xx,
Accepted 00th January 20xx

DOI: 10.1039/x0xx00000x

www.rsc.org/

Pin Tian,[a] Libin Tang*[a,b], Jinzhong Xiang*[a], Zhenhua Sun[c], Rongbin Ji*[b], Sin Ki Lai,[d] Shu Ping Lau,[d] Jincheng Kong[b], Jun Zhao[b], Chunzhang Yang[b] and Yanhui Li[b]

Solution processable high-performance, large-area, low-cost infrared organic photodetectors (OPDs) have been receiving more and more attention for their important applications both in scientific and technological fields. Looking for a simple method to upgrade device performance for OPDs becomes increasingly important. Here, the performance of OPDs in the near-infrared (NIR) region are tremendously improved by doping iodine into the device's active layer (P3HT:PCBM:I_2), 2.7 *wt*. % iodine doping may increase the absorption by 31.3% for the active film and result in the ~11000-fold increase in responsivity for the detector. A high detectivity (D^*) of $\sim 1.6\times10^{12}$ cmHz$^{1/2}$W^{-1} and a good specific responsivity (R) of ~80 AW^{-1} are achieved under the illumination (λ= 850 nm) at room temperature. The systematic characterizations reveal that iodine-doping can introduce acceptor states in the energy band gap for the polymer layer, and thus increase the harvesting to long wavelength photons. The small dose of iodine doping can significantly induce the improvement in device performance. This work demonstrates a simple but feasible method to enhance NIR optoelectronics device.

Introduction

Organic photodetectors (OPDs) have been intensively studied in recent years due to their numerous advantages including the low-cost of fabrication, light weight, high flexibility, compatibility for large area fabrications by means of roll-to-roll production or ink-jet printing.[1-7] Highly sensitive OPDs based on polymers and small molecules exhibiting a broad spectral ranges, and a detectivity of 7×10^{12} cmHz$^{1/2}$W^{-1} [8] in the visible light region, have been reported recently.[9,10] The blend of P3HT:PCBM has been widely used for active layer in organic solar cells (OSCs) achieved an efficiency up to 5%.[11] In spite of the promising performance, organic photodetectors (OPDs) based on P3HT:PCBM blend (PPB) is yet to be developed as a detectivity (D^*) reaching the order of 12 is rarely reported. In the present work, near infrared photodetectors based on iodine-doped P3HT:PCBM blend (IPPB) were fabricated. A high specific detectivity (D^*) and responsivity (R) over 1.6×10^{12}cmHz$^{1/2}$W^{-1} and 80 (AW^{-1}) respectively are achieved in these devices. The responsivity of IPPB device is 10^4 times higher than PPB. The mechanism for the enhancement resulted from iodine-doping is attributed to electron transfer from carbon to iodine due to the high electron affinity of iodine.

[a] *School of Materials Science and Engineering, Yunnan University, Kunming 650091, P.R. China.*
[b] *Kunming Institute of Physics, Kunming 650223, P.R. China.*
[c] *College of Optoelectronic Engineering, Shenzhen University, Shenzhen, 518000, P.R. China.*
[d] *Department of Applied Physics, The Hong Kong Polytechnic University, Hong Kong SAP, P.R. China.*

† Electronic supplementary information (ESI) available: The ellipsometric spectra of the doped and undoped P3HT:PCBM films. See DOI:

Experimental

Organic bulk heterojunction photodetectors (OPDs) in this study were prepared according to the following procedure: indium tin oxide (ITO) coated glass substrate used for bottom electrode (Hefei Kejing) was first cleaned by chemical bath method with mixed solution containing H_2O:H_2O_2:NH_3·H_2O (2:1:1) in the hot water at 80 °C for 30 min and then dried under air flow. Afterwards upon it a film of poly (3,4-ethylenedioxythiophene):poly(styrenesulfonate) (PEDOT:PSS) (Sigma-Aldrich) used for the hole transport layer was spin-coated with rotary speed of 2000 rpm for 60 s. The film of PEDOT:PSS was dried at 150 °C for 20 min.[12] The thickness of the PEDOT:PSS layer was approximately 96 nm. Next, P3HT(Sigma-Aldrich):PCBM(Jilin OLED) (1:0.8 weight ratio) or P3HT:PCBM:I_2 (Sinopharm Chemical)(1:0.8:0.05 weight ratio) (2.7 *wt*.% iodine doping) solution in chlorobenzene was spin-coated on top of the PEDOT:PSS layer with a rotary speed of 2000 rpm for 30 s, Then the sample was annealed at 150 °C for 30 min.[13] The thickness of polymer blend active layer was approximately 140 nm. To complete the OPD, aluminum (130 nm) electrodes acted as top electrodes were deposited by thermal evaporation under vacuum ($\sim 2.3\times10^{-4}$ Pa). Two kinds of devices with the structure ITO/ PEDOT:PSS/P3HT:PCBM/Al and ITO/PEDOT:PSS/P3HT: PCBM: I_2/Al were fabricated and the effective area of the devices are 0.09 cm^{-2}.

J-V curves were measured using Keithly 2400 sourcemeter. Photoresponse performance was measured at room temperature under illumination of a light emission diode (LED) with the wavelength of 850 nm at different power densities. Light passed from the ITO side. The cross-section of the device was characterized by Scanning Electron Microscope (SEM, FEG Quanta 650). The morphology of the active layer was observed using Atomic Force Microscopy (AFM, SPA-400). The photoluminescence characterization of the active layer was carried out using photoluminescence spectrometer (Hitachi F-4500). UV-Vis-NIR absorption spectra measurements were conducted in a nitrogen atmosphere using a Horiba iHR 320 spectrometer. The ellipsometric spectra were measured using JY Auto SE instrument. Chemical

bonding analysis of the active layer was carried out using X-ray photoelectron spectroscope (XPS, PHT VersaProbe Ⅱ With AES). The Raman spectra of the active layer were obtained by Renishaw in Via Raman microscope using 514.5 nm argon-ion laser. The Fourier transform-infrared (FT-IR) spectra of the active layer were acquired by a Thermo Nicolet Avatar 360 spectrometer using the KBr pellet technique.

Results and discussion

The structure of the devices in this study is shown in Fig. 1a. OPDs are commonly composed of a blend layer of a conjugated polymer (such as P3HT) as the donor and a fullerene derivative (such as PCBM) as the acceptor, which is sandwiched between a PEDOT:PSS-modified ITO as the positive electrode and a low work function metal as the negative electrode. Iodine is doped in the active layer with a fixed thickness. The cross section SEM image of a device based on an active layer without doping is shown in Fig. 1b. The thicknesses of each layer were determined as shown in Fig. 1b. The thicknesses of the films are consistent with previous reports.[14,15] Figs. 1c and 1d present the AFM topography images of PPB and IPPB films on silica glass, respectively. Their root-mean-squared (RMS) roughnesses were measured to be 8.9 nm and 10.3 nm, respectively. The difference in roughness of the doped and un-doped active layer is small, indicating a uniform distribution of iodine throughout the P3HT:PCBM layer .

Iodine doping adjusted the optical properties of PPB apparently. The optical properties of the spun PPB and IPPB films on quartz glass were measured and shown in Fig. 2. Iodine doping may drastically increased light absorption in UV-Vis-NIR range as shown in Fig. 2a, which may be clearly seen that doping may darken the active film (the inset of Fig. 2a). From the normalized UV-visible absorption spectra of the two films (see Fig. 2b), it is clearly to find that the absorption peak of the doped film has a red-shift of 12 nm. In the photoluminescence (PL) spectra (see Figs. 2c and 2e, respectively), the wavelengths of the strongest emission peak move towards longer wavelength with the increase of excitation wavelength for the doped film. However, this phenomenon does not appear for the un-doped film. It suggests that iodine-doping is more efficient in light absorption and PL emission for longer wavelength light. In Figs. 2d and 2f. The photoluminescence excitation (PLE) spectra of the IPPB film shows a peak wavelength at 384 nm, which is 4 nm red-shifted compared with PPB. The ellipsometric studies (see ESI) reveals that the absorption coefficient (α) of IPPB film is larger than PPB for the long wavelength light. Based on the above investigation, it can be concluded that iodine-doping can enhance the absorption of P3HT:PCBM films for the long wavelength light.

To get more insight into the effect of iodine-doping, Raman spectroscopy and Fourier transform-infrared (FT-IR) spectroscopy measurements were further carried out to characterize the molecular

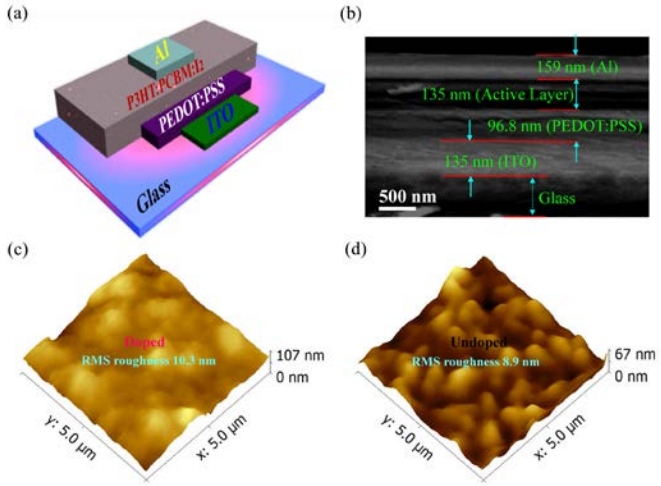

Fig.1 (a) The schematic diagram of the structure of organic photodetectors. (b) The SEM cross-section image of the P3HT:PCBM (1:0.8 weight ratio) based devices. (c) and (d) The AFM images of the P3HT:PCBM blend layers with and without iodine doping, respectively.

structure. Fig. 3a illustrates the Raman spectra of active films with or without doping, the Raman spectra of PPB film agrees with the results from Veerender and Gupta et al..[16] Various Raman modes are identified in the Raman spectra at 1449 cm^{-1} (symmetric C=C stretch mode), 1380 cm^{-1} (C-C intra-ring stretch mode).[17,18] It should be noted that the doped active film shows a red-shift of 2 cm^{-1} at 1449cm^{-1} （see the inset of Fig. 3a）, which indicates that iodine-doping affects the C=C stretch because the vibration peak of the C=C banding stretch is weakly varied. The FT-IR characterization on the as-deposited PPB and IPPB shows a similar trend, as shown in Fig. 3b, the band at 1555cm^{-1} is attributed to the stretching vibration of C=C in polymer.[19-21] While a red-shift of 2 cm^{-1} for the doped film is seen in the inset of figure. Both the Raman spectra and FT-IR spectra coherently prove that iodine has the effect on the stretching of C=C.

To shed light on that how the iodine atom influences C=C, the X-ray photoelectron spectroscopy (XPS) measurement was carried out to investigate the chemical bonding of the films. Fig. 3c is the full-scan XPS spectra of the BBP film (red) and the IPPB film (blue). Their high resolution C1s peaks are displayed in Figs. 3e and 3f, respectively. The C1s spectrum of PPB film reveals that it consists of three main components contributing to C=C (～284.6 eV), C-C (～285.5 eV) bonds and C-O (～ 286.5 eV).[22-38] After doped by iodine, the new C-I (～287.0 eV) [39] bond forms in the blend film. The above characterization proves the iodine-doping affect carbons by forming new chemical bonds, and thus changed the properties of C=C. This process is illustrated in Fig. 3d. The electronegativity of iodine (2.66) is bigger than that of carbon(2.55), thus iodine atom may attract electron that around carbon, leaving carbon positively charged. By transfer of electron from carbon to iodine, a new chemical bond (C-I) is formed. Therefore, the active layer doped by iodine will absorb the light with longer wavelength. Suming up the above characterizations, two important conclusions can be drawn.

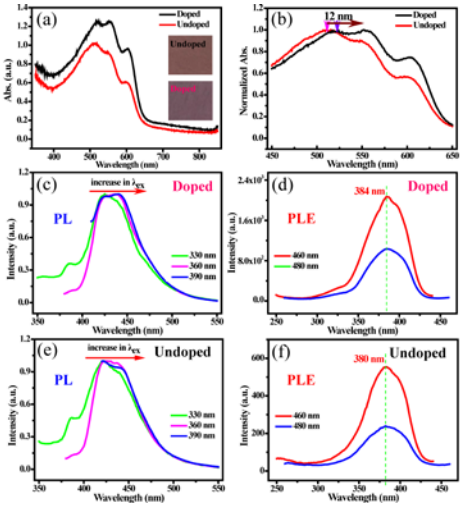

Fig. 2 (a) The UV-Vis-NIR absorption spectra of P3HT:PCBM and P3HT:PCBM:I_2 films, inset: the sample films spun-coated on quartz glass. (b) The normalized absorption spectra of (a). (c) and (e) The PL emission spectra of the blend films with and without doping, respectively. (d) and (f) The PL excitation spectra of the doped and undoped blend layers, respectively.

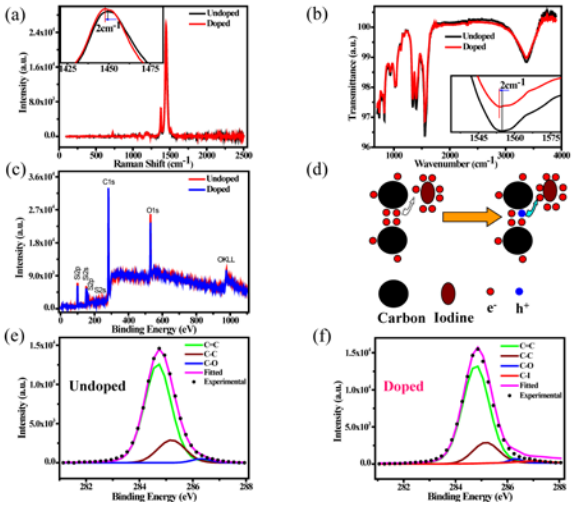

Fig. 3 (a) The Raman spectra of the doped and undoped active layers. Inset: the partial magnified Raman spectra. (b) The FT-IR spectra of the doped and undoped active films. Inset: the partial magnified FT-IR spectra. The Full-scan(c), C1s (undoped) (e) and C1s (doped) (f) XPS spectra of the samples. (d)The schematic diagram of the iodine doping mechanism.

Firstly, the doping of iodine is effective and it induces *p*-type doping in IPPB. Secondly, iodine has a huge effect on the optical modification of IPPB due to its big electronegativity.

Iodine doping may tremendously upgrade device performance. Both iodine doped (IPPB) and undoped (PPB) OPV detectors have been fabricated. Figs. 4a/b and c/d show the *J-V* curves of devices with and without doping, respectively. The curves are measured under the illumination of an LED at a wavelength of 850 nm with different power densities. The *J-V* characteristics of organic photodetectors is given by eqn. (1), which is based on the thermionic emission theory ,[40-41]

$$J = J_0[\exp(\frac{qV}{nk_0T}) - 1] \quad (1)$$

where J_0 is the reverse saturated current density, T the temperature, q unit charge, V the applied voltage, k_0 Boltzman constant and n is the ideal factor related to the slope. J_0 can be described by eqn. (2), which is obtained by extrapolating the logarithmic *J-V* curves,

$$J_0 = A^* T^2[\exp(\frac{-q\Phi_B}{k_0T}) - 1] \quad (2)$$

where A^* is the Richardson constant, which is defined as $A^* = \frac{4\pi m^* k_0^2}{h^3}$, where m^* is the effective mass, h and Φ_B are Planck's constant and the barrier height, respectively. For the blend layer of P3HT and PCBM with the weight ratio of 1:0.8, the effective mass is 1.7 m_e (free electron mass).[42] The electron mass for P3HT and PCBM doped with iodine is calculated by eqn. (3), [43]

$$m^* = m^*(\text{P3HT:PCBM})\omega(\text{P3HT:PCBM}) + m^*(I_2)\omega(I_2) \quad (3)$$

where ω (P3HT:PCBM) and ω (I_2) are mass fractions for P3HT:PCBM (1:0.8 weight ratio) and iodine respectively. For iodine, the effective electron mass is 2.4 m_e.[44] As the doped iodine in active layer is 0.01 *at.*%, it can assume that the effective mass for the doped blend film approximately remains ~1.7 m_e. The logarithmic plots of the *J-V* curves display a linear region under the forward bias. [45] We can extract J_0 and n for each device under different power densities from the Figs. 4b and 4d. According to eqn. (2), the Φ_B and n under various conditions were obtained and listed in Table 1.

Table 1 The ideality factors (n) and barrier heights (Φ_B) for the doped and undoped devices under different power intensities.

Device	Working conditions		n	Φ_B (eV)
Undoped	Dark		2.85	0.86
	Light Intensity (mWcm^{-2})	0.11	1.84	1.50
		0.67	0.83	1.23
Doped	Dark		1.37	0.94
	Light Intensity (mWcm^{-2})	0.11	1.36	0.93
		0.67	1.44	0.79

By comparing Figs. 4b and 4d, it can be seen that under the light condition, the change in current density for the doped device is about two orders of magnitude larger than that in the dark, while this change is little for the undoped device (Fig. 4d). It should be noted that for the doped device the lowest current densities are at around

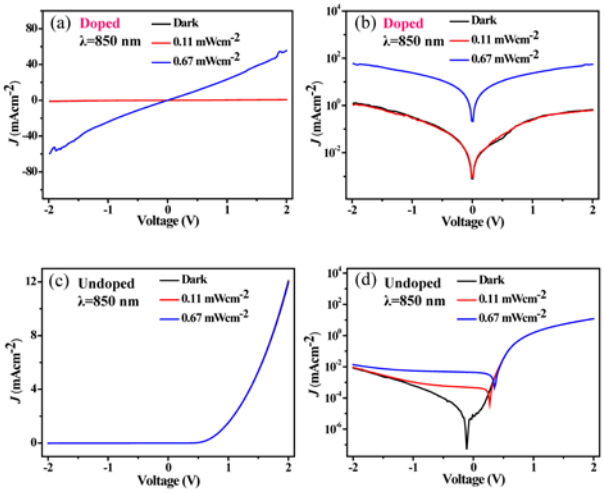

Fig. 4 (a) and (c) The *J-V* characteristics of the devices with or without iodine doping, respectively. (b) and (d) The Logarithmic *J-V* curves of the doped or undoped devices, respectively. The curves are measured under the NIR LED (λ=850 nm) illumination with different power densities.

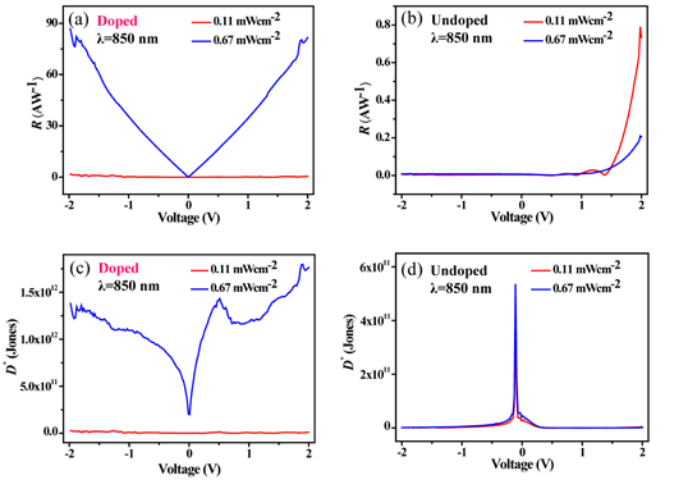

Fig. 5 (a) and (b) The bias voltage dependent responsivity (*R*) of the doped and undoped devices, respectively. (c) and (d) The bias voltage dependent detectivity (D^*) of the doped and undoped devices, respectively. The performances of the devices are measured at room temperature.

zero bias voltage both in the dark and under illumination. For the undoped device, however, the voltage values at the lowest current density do not remain constant, they move to the positive values with the power density increasing.

An important figure of merit for an OPD[46] is the responsivity (*R*) which is given by eqn. (4):

$$R = J_{ph} / P_{opt} \tag{4}$$

where J_{ph} is photocurrent which equals to the absolute value of the current density under illumination subtracting that in the dark, P_{opt} is the incident optical power. Another important figure of merit is the detectivity, D^*, which is expressed as eqn. (5):[47]

$$D^* = R / \sqrt{2q|J_{dark}|} \tag{5}$$

where J_{dark} is the dark current density, q the unit charge. According to the *J-V* characteristics, we can calculate the *R* and D^*. The curves of *R* and D^* *vs.* applied voltage of the OPDs are shown in Fig. 5.

From Figs. 5a and 5b it can be seen that the *R* of the doped device is two orders of magnitude higher than that of the undoped. Comparing the above two figures, it is observed that the undoped device just displays a higher responsivity at the positive bias instead of both the negative and positive bias for the doped device. Figs. 5c and 5d show that the D^* of the doped device is an order of magnitude higher than the undoped. The applied voltage dependent D^* curves for the doped and undoped devices show a nearly opposite trend. This can be explained through eqns. (4) and (5). D^* depends on the synergism of *R* and J_{dark} of the devices. Thus, the variation of *R* and J_{dark} with the bias will intensively influence the relationship of D^* and bias. Importantly, a small dose of iodine doping may tremendously increases the *R* and D^* for OPV detector, moreover, it can be deduced that a proper dose of iodine doping could also upgrade the OPV solar cells for the increase in current density under illumination induced by the increased light absorption.

Conclusion

In this work, for the first time we report the performance enhancement of organic photodetectors based on P3HT: PCBM using iodine doping. The devices based on iodine-doped P3HT: PCBM blend shows a high detectivity up to 1.6×10^{12} cmHz$^{1/2}$W^{-1} in the NIR region. The good performances are attributed to the iodine doping. As a material with broad absorption spectral range, this method of doping iodine into the active layer of P3HT and PCBM opens up the possibility for fabricating high-performance, lost-cost, large-array IR OPDs. Moreover, a proper dose of iodine doping should also be important for upgrading the performance of the OPV solar cells for the increased light absorption.

Acknowledgements

This work was supported by National Natural Science Foundation of China (No. 61106098), and the Key Project of Applied Basic Research of Yunnan Province, China (No. 2012FA003).

Notes and references

1 T. Rauch, M. Boberl, S.F. Teddle, J. Furst, M.V. Kovalenko, G.N. Hesser, U. Lemmer, W. Heis and O. Hayden, *Nat. Photonics*, 2009, **3**, 332-336.
2 F.C. Krebs, S.A. Gevorgyan and J.A. Alstrup, *J. Mater. Chem.* , 2009, **19**, 5442-5451.
3 F.C. Krebs, *Energy Mat. Sol. Cells*, 2009, **93**, 394-412.
4 Y. Yao, Y.Y. Liang, V. Shrotriya, S.Q. Xiao, L.P. Yu and Y. Yang, *Adv. Mater.* , 2007, **19**, 3979-3983.

5 G.J. Matt, T. Fromherz, M. Bednorz, S. Zamiri, G. Goncalves, C. Lungenschmied, D. Meissner, H. Sitter, N.S. Sariciftci, C.J. Brabec and G. Bauer, *Adv. Mater.* , 2010, **22**, 647-650.
6 S.C.J. Meskers, J.K.J. van Duren, R.A.J. Janssen, F. Louwet and L. Groenendaal, *Adv. Mater.* , 2003, **15**, 613-616.
7 G. Yu, K. Pakbaz and A.J. Heeger, *Appl. Phys. Lett.* , 1994, **64**, 3422-3424.
8 M. Ramuz, L. Bürgi, C. Winnewisser and P. Seitz, *Org. Electron.* , 2008, **9**, 369-376.
9 X. Gong, M.H. Tong, Y,J. Xia, W.Z. Cai, J.S. Moon, Y. Cao, G. Yu, C.l. Shieh, B. Nilsson and A.J. Heeger, *Science*, 2009, **325**, 1665-1667.
10 M.S. Arnold, J.D. Zimmerman, C.K. Renshaw, X. Xu, R. R. Lunt, C.M. Austin and S.R. Forrest, *Nano Lett.* , 2009, **9**, 3354-3358.
11 M. Reyes-Reyes, K. Kim, J. Dewald, R. Lopez-Sandoval, A. Avadhannla, S. Curran and D.L. Carroll, *Org. Lett.* , 2005, **7**, 5749-5752.
12 B.T.de Villers, C.J. Tassone, S.H. Tolbert and B.J. Schwartz, *J. Phys. Chem. C*, 2009, **113**, 18978-18982.
13 S.R. Gollu, R. Sharma, G. Srinivas, S. Kundu and D. Gupta, *Org. Electron.* , 2014, **15**, 2518-2525.
14 P. Kubis, L. Lucera, F. Machui, G. Spyropoulos, J. Cordero, A. Frey, J. Kaschta, M.M. Voigt, G.J. Matt, E. Zeira and C.J. Brabec, *Org. Electron.* , 2014, **15**, 2256-2263.
15 S.-T. Chuang, S.-C. Chien and F.-C. Chen, *Appl. Phys. Lett.* , 2012, **100**, 013309.
16 P. Veerender, V. Saxena, A.K. Chauhan, S.P. Koiry,P. Jha, A. Gusain, S. Choudhury, D.K. Aswal and S.K. Gupta, *Sol. Energy & Sol. Cells*, 2014, **120**, 526-535.
17 W.C. Tsoi, D.T. James, J.S. Kim, P.G. Nicholson, C.E. Murphy, D.D.C. Bradley, J. Nelson and J.-S. Kim, *J. Am. Chem. Soc.* , 2011, **133**, 9834-9843.
18 A.M. Ballantyne, T.A.M. Ferenczi, M. Campoy-Quiles, T.M. Clarke,A. Maurano, K.H. Wong, W.M. Zhang, N. Stingelin-Stutzmann, J.-S. Kim, D.D.C. Bradley, J.R. Durrant, I. McCulloch, M. Heeney, J. Nelson, S. Tierney, W. Duffy, C. Mueller and P. Smith, *Macromolecules*, 2010, **43**, 1169-1174.
19 J.Y. Oh, M. Shin, H.W. Lee, Y.-J. Lee, H.K. Baik and U. Jeong, *ACS Appl. Mater.* , 2014, **6**, 7759-7765.
20 M.H. Li, Z.X. Liu, J.L. Ruan, X. Chen, F.D. Xu, X. Chen, X. Lu and S.F. Yang, *RSC Adv.* , 2014, **4**, 53999-54006.
21 R.K. Singh, J. Kumar, A. Kumar, V. Kumar, R. Kant and R. Singh, *Sol. Energy & Sol. Cells*, 2010, **94**, 2386-2394.
22 H.-J. Shin, K.K. Kim, A. Benayad, S.-M. Yoon, H.K. Park, I.-S. Jung, M.H. Jin, H.-K. Jeong, J.M. Kim, J.-Y. Choi and Y.H. Lee, *Adv. Funct. Mater.* , 2009, **19**, 1987-1992.
23 X. Wang, L.J. Zhi and K. Müllen, *Nano Lett.* , 2008, **8**, 323-327.
24 S. Watcharotone, D.A. Dikin, S. Stankovich, R. Piner, I. Jung, G.H.B. Donmett, G. Evmenenko, S.-E. Wu, S.-F. Chen, C.-P. Liu, S.T. Nguyen and R.S. Ruoff, *Nano Lett.* , 2007, **7**, 1888-1892.
25 J.T. Robinson, F.K. Perkins, E.S. Snow, Z.Q. Wei and P.E. Sheehan, *Nano Lett.* , 2008, **8**, 3137-3140.
26 D.W. Wang, F. Li, J. Zhao, W. Ren, Z.G. Chen, J. Tan, Z.-S. Wu, I. Gentle, G.Q. Lu and H.-M. Cheng, *ACS Nano*, 2009, **3**, 1745-1752.
27 G. Eda, G. Fanchini and M. Chhowalla, *Nat. Nanotech.* , 2008, **3**, 270-274.
28 K.S. Novoselov, D. Jiang, F. Schedin, T.J. Booth, V.V. Khotkevich, S.V. Morozov and A.K. Geim, *Proc. Natl. Acad. Sci. USA*, 2005,**102**: 10451-10453.
29 K.S. Novoselov, A.K. Geim, S.V. Morzov, D. Jiang, Y. Zhang, S.V. Dubonos, I.V. Grigorieva and A.A. Frisov, *Science*, 2004, **306**, 666-669.
30 C. Berger, Z. Song, T. Li, X. Li, A.Y. Ogbazghi, R. Feng, Z. Dai, A.N. Marchenkov, E.H. Conrad, P.N. First and W.A.de Heer, *J. Phys. Chem. B*, 2004,**108**, 19912-19916.
31 K.S. Kim, Y. Zhao, H. Jang, S.Y. Lee, J.M. Kim, K.S. Kim, J.-H. Ahn, P. Kim, J.-Y. Choi and B.H. Hong, *Nature*, 2009, **457**, 706-710.
32 D.W. Boukhvalov and M.I. Katsnelson, *J. Am. Chem. Soc.* , 2008, **130**, 10697-10701.
33 K.A. Mkhoyan, A.W. Contryman, J. Silcox, D.A. Stewart, G. Eda, C. Mattevi, S. Miller and M. Chhowalla, *Nano Lett.* , 2009, **9**, 1058- 1063.
34 S. Gilje, S. Han, M. Wang, K.L. Wang and R.B. Kaner, *Nano Lett.* , 2007, **7**, 3394-3398.
35 X. Li, H. Wang, J.T. Robinson, H. Sanchez, G. Diankov and H. Dai, *J. Am. Chem. Soc.* , 2009, **131**, 15939-15944.
36 H. Wang, J.T. Robinson, X. Li, H. Dai, *J. Am. Chem. Soc.* , 2009, **131**, 9910-9911.
37 X. Fan, W. Peng, Y. Li, X. Li, S. Wang, G. Zhang and F. Zhang, *Adv. Mater.* , 2008, **20**, 4490-4493.
38 S. Stankovich, D.A. Dikin, R.D. Piner, K.A. Kohlhaas, A. Kleinhammes, Y. Jia, Y. Wu, S.T. Nguyen and R.S. Ruoff, *Carbon*, 2007, **45**, 1558-1565.
39 S. Hoste, D.F. Van De Vondel and G.P. Van Derkelen, *J. Electron. Spectrosc. Relat. Phenom.* , 1979, **17**, 191-195.
40 L.J.A. Koster, E.C.P. Smits, V.D. Mihailetchi and P.W.M. Blom, *Phys. Rev. B. Condens. Matter. Phys.* , 2005, **72**, 085205.
41 C.R. Crowell, *Solid-State Electron.* , 1965, **8**, 395-399.
42 P.D. Cunninghan and L.M. Hayden, *J. Phys. Chem C*, 2008, **112**, 7928-7935.
43 J. Zhao, L.B. Tang, J. Xiang, R. Ji, Y. Hu, J. Yuan, J. Zhao, Y. Tai and Y. Cai, *RSC Adv.* , 2015, **5**, 29222-29229.
44 Y. Natsume and T. Suzukl, *Solid State Commun.* , 1982, **44**, 1105-1107.
45 S. Tongay, M. Lemaitre, X. Miao, B. Gila, B.R. Appleton and A.F. Hebard, *Phys. Rev. X*, 2012, **2**, 011002.
46 W. Lv, Y. Peng, J. Zhong, X. Luo, Y. Li, T. Zheng, Y. Tang, L. Du and L. Peng, *IEEE Photonics Technology Letters*, 2015, 2449631.
47 X. Wang, H. Li, Z. Su, F. Fang, G. Zhang, J. Wang, B. Chu, X. Fang, Z. Wei, B. Li and W. Li, *Org. Electron.* , 2014, **15**, 2367-2371.

A high-performance IR OPV detector has been fabricated, 2.7 *wt*. % iodine doping may increase the absorption by 31.3% for the active film thus result in the ~11000-fold increase in responsivity for the detector.